JAST
Journal of Aerospace Science and Technology

Pages: 61-71/ Vol. 15/ No. 2 / Summer- Fall 2022

Journal of Aerospace Science and Technology

www:jast.ias.ir

Scientific-Research Article

Droplet Breakdown Analysis inside Porous Media at Different Porosities, Using LBM

Mohammad Reza Salimi[1]*, Mohammad Taeibi Rahni [2], Abolfazl Amiri Hezaveh[3], Mahdi Zakyani Roudsari Amir[4]

1-4- Aerospace Research Institute, Tehran, Iran Electerical
2- Sharif University of Technology, Tehran, Iran
3- Department of Mechanical Engineering, Islamic Azad University Central Tehran Branch, Tehran, Iran

ABSTRACT

Keywords: Porous media; Pore-scale; Two-phase Flow; Droplet; Lattice Boltzmann Method

In present research, the interaction between single liquid droplet with particles inside a porous media is investigated numerically in two dimensions. The He's model is used to simulate two phase flow and multiple relaxation time collision operator is implemented to increase numerical stability. Simulations have performed in three non-dimensional body forces of 0.000108, 0.000144, 0.000180, porosity values of 0.75, 0.8, 0.85 and Ohnesorge range of 0.19-0.76. In the range of investigated non-dimensional parameters, two distinct physics of droplet trapping and break up have observed. The related results revels that for every values of investigated non-dimensional body forces and porosity, there is a critical Ohnesorge number that droplet breaks up occurs for larger values. This critical value decreases as non-dimensional body force and porosity increases. Based on these results, a droplet trapping or break up behavioral diagram is drown with respect to the investigated density ratio, Ohnsorge, Reynolds and Capilary numbers.

Introduction

The study of flow in porous media has always been of interest to researchers. In nature and technology, we see many phenomena that are somehow related to porous media. Water filtration in rocks, fluid flow among underground rocks and underground aquifers are specific examples of this physics. In oil engineering, the rocks of an oil field can be considered as a porous media. In this field of research, understanding the behavior of fluids in natural reservoirs, knowing the amount of oil or oil derivatives are among the technical parameters that should be considered in the design of an extraction system. Therefore, the study of the two-phase fluids flow of oil in reservoirs has been the subject of extensive researches [1-2].

Among the more modern applications related to porous media, we can mention the investigation of two-phase flow in the electrodes of fuel cells [3]. In biotechnology, trees and plants can draw and

1 Assistant Professor (Corresponding Author) **Email:** *mohammadsalimi@ari.ac.ir
2 Professor
3 Msc
4 Assistant Professor

DOI: 10.22034/jast.2022.322220.1110
Submit: 31.11.2021/ Accepted: 10.04.2022
Print ISSN:1735-2134 Online ISSN: 2345-3648

transfer water through the hollow structures inside their stems and leaves due to high capillarity. In addition, many biological membranes can be considered as porous media, which is an explanation and a reason for the development of theories related to porous media in the field of biotechnology [4-5].
As can be seen, the interaction of two-phase flow with porous media is widely used in various industries and nature. Therefore, in this field, fundamental studies of the phenomena and the physics are needed. Thus, the subject of the present research is the detailed investigation of the interaction of droplets with the internal structure of the porous medium and the identification of related phenomena.
In classical theories of simulating porous media, the effects of porous substance on fluid flow and transfer phenomena are considered through source terms. In this way, the governing equations of the fluid dynamics inside the porous medium are modified by the source terms. This type of macro-scale analysis is based on volume averaging of the effects of the porous medium.
The Darcy relation, which was presented by Henry Darcy in the 19th century, is based on the macroscale approach. This relationship states that in the steady state, the mass flow rate of the fluid inside the porous medium is proportional to the ratio of the pressure difference and the dynamic viscosity of the fluid. The proportionality constant of this relationship is the most important quantity in the porous medium, which is called permeability. The permeability of a porous medium largely depends on the size, distribution and shape of pore structures.
Darcy's law is only valid for Newtonian fluids at very low Reynolds numbers. As the fluid flow rate increases, the deviation from Darcy's law increases. This subject was first reported by Forchheimer, 1901. Experimental observations and mathematical models show that this deviation is dependent on the effects of inertia, turbulence and other factors that can be attributed to the high flow speed.
Hubert pointed out in 1956 that the deviation from Darcy's law occurs at a Reynolds number close to 1 (based on the size of the grains that make up the porous medium), while the turbulence phenomenon does not become important until Reynolds number of about 600 (Aziz and Settari, 1979). A modification of the Darcy equation for flow at high Reynolds is applied by the second-order Forchmeier term.
In order to calculate the permeability, relationships have been developed that provide the possibility of estimating this quantity based on the geometric properties of the porous medium. An example of these equations is the Kozeny-Carman equation, which relates permeability to the porosity, the shape factor, and a quantity called Tortuosity [1].
In the case of multiphase flows in porous media, the Darcy relation can be developed by the concept of relative permeability, which is an attempt to include the effects of the presence of other fluids (in the form of a new phase). In this case, the wettability conditions of the porous medium and the dimensionless parameters related to the presence of the second phase are of great importance. The complexities of the subject caused that many fundamental works have been done (mainly experimentally) on the effect of different parameters on permeability or relative permeability inside porous media.
Pan et al. used the Lattice Boltzmann method with various collision operators to study the flow inside two porous media consisting of a regular arrangement of solid squared section particles and a random arrangement of circular solid particles [6]. It should be noted that their studies are single-phase. In general, the production of a porous medium through the random arrangement of particles is a common method and is observed in many articles. For instant, Aaltosalmi in 2005, used this configuration to study the permeability of pebbles made of sandstone [7]. Rostamzadeh et al. investigated the permeability coefficient of a two-dimensional porous media in high Knudsen numbers (slip flow regime) [8-9].
In the two-phase mode, Gunstensen et al. numerically investigated the two-phase flow inside a porous medium in three-dimensions. Their study was focused on high and low viscosity coefficients and porous media with a high percentage of saturation by the main phase. They presented their results in the form of various diagrams to classify the behavior of two-phase flow in porous media [10].
Ferreol et al. investigated single and two phase flows through a porous bed consisting of sandstone in three dimensions. They studied the sensitivity of calculated permeability on different parameters including, the sample size and model parameters [11]. Martys et al. numerically investigated a multi-material flow in a three-dimensional porous bed consisting of sandstone using LBM and Shan and Chen model. In their research, the replacement of one phase with another phase is well modeled and the relative permeability for different wetted phases

has been calculated. The results of their simulations are in good agreement with the experimental data [12]. Tölke et al. investigated a multiphase flow in a porous medium with variable viscosity and density ratio based on the model proposed by Gunstensen. In their research, the limitations and problems of the Lattice Boltzmann method were investigated in real problems [13].

Lin et al. investigated a real porous medium produced by X-ray Microtomography using LBM and the He model [14]. They used this model to simulate the purification process of two-phase fluid through a porous bed. Different surface tensions and low density ratios were investigated in this study [15].

Frank, and Perré studied the impact of a droplet on the surface of a porous medium at different porosity and contact angles. They results showed a power law behavior with respect to time for the radius of the wetted area inside the porous medium, whose constants depend on the porosity coefficient of the medium [16].

Using Shan and Chen's single-component model [17], Huang et al. studied the dependence of relative permeability on various parameters such as contact angle and viscosity ratio in a random arrangement of two-dimensional squares obstacles [18]. Shan and Chen's two-component model was used before by Pan et al. to obtain the capillary pressure saturation curve and compare it with experimental data [19]. Hao, and Cheng also used the free energy method to calculate the relative permeability of a bunch of spheres [20]. Tabe et al. investigated the two-dimensional flow of condensed water and steam mixture in a fuel cell polymer electrolyte membrane using the Lattice Boltzmann method [21]. Huang et al. also studied the two-phase fluid flow inside porous medium using the Lattice Boltzmann method and the color gradient model with multiple relaxation times collision operator [22].

Huan et al. compared three free energy models, Shan & Chen and Rothman-Keller, in terms of accuracy and numerical stability for simulating two-phase flow inside a porous medium [23]. Their study showed that Rothman-Keller and free energy models have better accuracy at high viscosities. Additionally, in terms of accuracy and stability, these two models perform much better than Shan & Chen model. Liu et al. also used LBM along with the Lee model to study the two-phase flow inside porous medium [24]. Latifiyan et al. investigated the evaporation of droplets in contact with a porous medium and studied different dimensionless numbers related to multiphase flow, heat transfer and porous geometry. They investigated the temperature, flow and mass transfer profiles [25]. Taghilu and Rahimian analyzed the penetration process of very large droplet into a porous medium consisting of a random arrangement of particles in two dimensions, using LBM and Shan & Chen two-phase model. They investigated the effects of surface wettability and Darcy number on drop penetration [26]. In a similar study, SalehAbadi et al. analyzed the penetration of liquid film and droplet inside the porous medium using Shan & Chen model. They simulated viscous fingering and capillary fingering permeation regimes for a porous medium consisting of hydrophilic and hydrophobic particles [27]. Note, in the above mentioned researches, there is a significant difference between the length scales of the droplets and the particles of the porous medium. This is the most important difference between the above works and the current research, in which the length scale of the droplet and the particles of the porous medium is the same. Rastegar Rajeouni and Rahmati studied the effect of the electric field on the droplet behavior in the porous medium in two dimensions, using LBM. They used He–Chen–Zhang phase field model to analyze the two-phase flow. It should be noted that in their research, the porous medium was not analyzed at the pore scale [28].

It is clear that, in none of the above mentioned studies, the behavior of a single droplet of the same scale as the porous medium pores has not been studied. in some of these researches, the droplet radius is much larger than the size of the particles. This large difference in the scale of droplets and particles of the porous medium causes the particles to penetrate the droplets instead of breaking them. Therefore, in the current research, the length scales of the droplets and the porous medium particles are considered to be at the same order, which results in more diversity in the behavior of the droplets breaking in the porous medium. In other words, the same scale of droplets and obstacles in the porous medium caused the occurrence of various phenomena that are reported in the present research. In addition, in present research, an attempt has been made to define dimensionless numbers with indicators that can be measured on a macroscopic scale. This helps to produce meaningful non-dimensional parameters from the point of view of

engineering (for example, the velocity scale is considered equal to the average speed in the porous medium). This also helps to generalizing the results. Based on our results, different diagrams have been extracted that can be very useful for predicting droplet dynamic behavior in porous media.

Problem Statement

In the present research, the two-phase flow inside a porous medium is investigated at pore scale. The geometry of problem is depicted in Fig. (1). As shown in this figure, due to the repetitive structure of the studied geometry, only one representative volume is analyzed in order to reduce the computational costs. In fact, by repeating this geometry, the entire porous medium is reconstructed. Therefore, as shown in Fig. (1), the boundary conditions of the problem are entirely periodic.

The flow regime is determined according to the flow Reynolds number. The fluid is under the influence of a specific body force, which is the main driver of its movement along the horizontal axis. The range of studied Reynolds numbers is from 2 to 16. Therefore, the studied flow is not within the Darcy regime.

The kinematic viscosity of both phases is assumed to be equal, but the densities are different. The kinematic viscosity of the main phase is 0.166666. Two density ratios of 1:2 and 1:3 have been investigated, and in both cases, the density of the main phase is 1. Thus, the density of the droplet changes.

The dimensionless numbers investigated in this research are Reynolds, Capillary and Ohnesorge, whose definitions are given in relations (1) to (3), respectively. In total, 60 simulations have been performed in the form of two density ratios, three dimensionless body forces and 10 Ohnesorge numbers.

$$\mathrm{Re} = \frac{\rho U D_{Pore}}{\mu}. \qquad (1)$$

In Eq. (1), U represents the average velocity of the fluid, D is the flow inlet width, ρ is the density, and μ is the dynamic viscosity.

$$Ca = \frac{U\mu}{\sigma}. \qquad (2)$$

Where, σ represents the surface tension. Capillary number represents the effect of the main phase on the secondary phase (droplet).

$$ohn = \frac{\mu}{\sqrt{\rho\sigma D}}. \qquad (3)$$

Ohnesorge number expresses the cohesion of the droplet. The porosity coefficient is also defined as the ratio of the volume (in two-dimensions the surface) V_f containing the fluid to the total volume (surface) V_{total}.

$$\varepsilon = \frac{V_f}{V_{total}}. \qquad (4)$$

Governing equations and boundary conditions

The equations of LBM distribution functions of incompressible isothermal two-phase flow are represented at equations of (5) and (6):

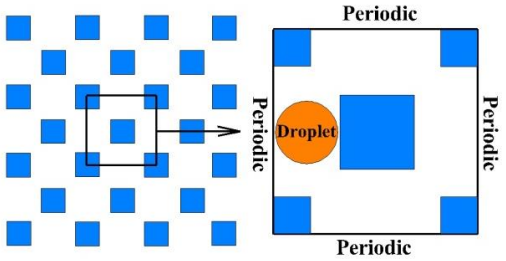

Figure 1: Schematic of problem geometry and boundary conditions.

$$\frac{Dg}{Dt} = -\frac{g - g^{eq}}{\lambda} - (\xi - u).[(\Gamma(u)(F_s + G) - (\Gamma(u) - \Gamma(0))\nabla\psi(\rho)], \qquad (5)$$

$$\frac{Df}{Dt} = -\frac{f - f^{eq}}{\lambda} - \frac{(\xi - u).\nabla\psi(\phi)}{RT}\Gamma(u), \qquad (6)$$

In which the first distribution function, g is used to calculate the flow quantities and f is used to trace the interface of two phases. The equilibrium distribution functions are also calculated as follows:

$$g^{eq} = \rho RT\Gamma(u) + \psi(\rho)\Gamma(0), \qquad (7)$$

$$f^{eq} = \varphi\Gamma(u). \qquad (8)$$

The parameters in equations (6 and 7) are defined as follows:

$$\Gamma(u) = \frac{1}{(2\pi RT)^{D/2}}\exp\left[-\frac{(\xi - u)^2}{2RT}\right], \qquad 9$$

$$\phi = \int f d\xi, \quad 10$$

$$p = \int g d\xi, \tag{11}$$

$$\rho RTu = \int \xi g d\xi. \tag{12}$$

The thermodynamic properties such as density and viscosity are calculated using equation (13).

$$\upsilon(\phi) = \upsilon_l + \frac{\phi - \phi_l}{\phi_h - \phi_l}(\upsilon_h - \upsilon_l). \tag{13}$$

The above equations have been discretized and analyzed on the standard volume specified in Figure (1). As shown in this figure, the periodic boundary condition is used on all four sides of the computational domain. The effect of solid boundaries has also been included in the calculations using the half-way bounce back method, which represents the no-slip boundary condition.

Discretization of Equations

The particle distribution function in D2Q9 model is discretized as follows [14].

$$e_\alpha = \begin{cases} 0, & \alpha = 0, \\ (\cos[\frac{(\alpha-1)\pi}{2}],\ \sin[\frac{(\alpha-1)\pi}{2}])C & \alpha = 1,2,3,4, \\ \sqrt{2}(\cos[\frac{(\alpha-5)\pi}{2}+\frac{\pi}{4}],\ \sin[\frac{(\alpha-5)\pi}{2}+\frac{\pi}{4}])C & \alpha = 5,6,7,8. \end{cases} \tag{14}$$

In which, c is equal to one. Based on the above discretization, the equilibrium distribution functions of flow and phase interface equations are written as follows:

$$\begin{aligned} g_\alpha{}^{eq} &= \omega_\alpha \left[p + \rho(\frac{3e_\alpha.u}{c^2} + \frac{9(e_\alpha.u)^2}{2c^4} - \frac{3u^2}{2c^2}) \right], \\ f_\alpha{}^{eq} &= \omega_\alpha \phi \left[1 + \frac{3e_\alpha.u}{c^2} + \frac{9(e_\alpha.u)}{2c^4} - \frac{3u^2}{2c^2} \right]. \end{aligned} \tag{15}$$

In which, the weight coefficients ω_a are defined as follows:

$$\omega_0 = 4/9,\ \omega_{1:4} = 1/9,\ \omega_{5:9} = 1/36 \tag{16}$$

To keep the method explicit, intermediate variables $\bar{f}_\alpha$ and $\bar{g}_\alpha$ are defined as follows:

$$\bar{f}_\alpha = f_\alpha + \frac{(e_\alpha - u).\nabla\psi(\phi)}{2RT}\Gamma_\alpha(u)\delta_t, \tag{17}$$

$$\bar{g}_\alpha = g_\alpha - \frac{1}{2}(e_\alpha - u).[\Gamma_\alpha(u)(F_s + G) - (\Gamma_\alpha(u) - \Gamma_\alpha(0))\nabla\psi(\rho)]\delta_t,$$

where δt is the time step and Γ_α (u) is defined as follows:

$$\Gamma_\alpha(u) = \omega_\alpha \left[1 + \frac{3e_\alpha.u}{c^2} + \frac{9(e_\alpha.u)^2}{2c^4} - \frac{3u^2}{2c^2} \right]. \tag{18}$$

The new variables $\bar{f}$ and $\bar{g}$ satisfy the transfer relations (19).

$$\begin{aligned} &\bar{f}_\alpha(x + e_\alpha\delta_t, t + \delta_t) - \bar{f}_\alpha(x,t) = -\frac{\bar{f}_\alpha(x,t) - f^{eq}{}_\alpha(x,t)}{\tau} \\ &-\frac{(2\tau-1)}{2\tau}\frac{(e_\alpha - u).\nabla\psi(\phi)}{RT}\Gamma(u)\delta_t, \\ &\bar{g}_\alpha(x + e_\alpha\delta_t, t + \delta_t) - \bar{g}_\alpha(x,t) = -\frac{\bar{g}_\alpha(x,t) - g^{eq}{}_\alpha(x,t)}{\tau} \\ &-\frac{(2\tau-1)}{2\tau}(e_\alpha - u).[\Gamma_\alpha(u)(F_s + G) - (\Gamma_\alpha(u) \\ &-\Gamma_\alpha(0))\nabla\psi(\rho)]\delta_t, \end{aligned} \tag{19}$$

Macroscopic quantities can also be calculated using the following relations:

$$\begin{aligned} \phi &= \sum \bar{f}_\alpha, \\ p &= \sum \bar{g}_\alpha - \frac{1}{2}u.\nabla\psi(\rho)\delta_t, \\ \rho RTu &= \sum e_\alpha \bar{g}_\alpha + \frac{RT}{2}(F_s + G)\delta_t. \end{aligned} \tag{20}$$

One of the most important issues in the numerical solution of two-phase flows is the correct distribution of density across the interface. In nature, the thickness of the interface between two fluids is zero, but in all the interface capturing numerical methods, several computational nodes are involved in the interface. In many studies of two-phase flows conducted by the Lattice Boltzmann method, the examination of the thickness of the interface is considered as a criterion for the grid independency study [29-31]. In this regard, the density distribution across the two-phase interface for three grid resolutions is shown in Figure (2). By looking at the diagrams, it is clear that the grid independent solution is obtained at the 141x141 lattice nodes.

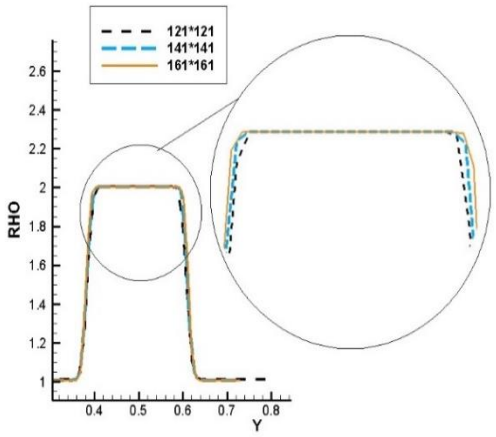

Figure 2: Density distribution in the droplet center line along the Y axis

Code Validation

In order to validate the results, two problems of Laplace's law and two-phase Poiseuille flow have been studied. In Laplace's law problem, a single drop that is not affected by any external force is simulated. After the drop is balanced, the pressure difference between inside and outside of it for different values of surface tension should change according to Eq. (21). Figure (3) compares the results of the current numerical model for two values of surface tension and three different drop radii with Eq. (21). As shown in this figure, there is a very good agreement between the results.

$$P_{Out} - P_{In} = \frac{2\sigma}{r} \tag{21}$$

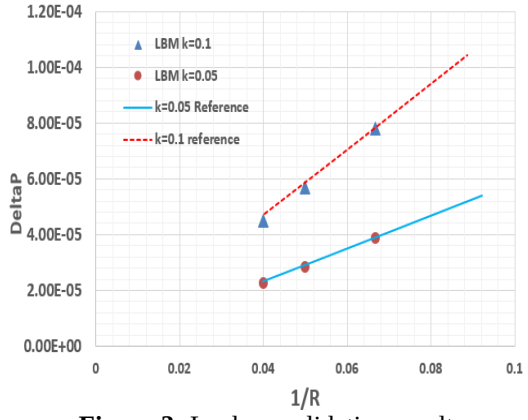

Figure 3: Laplace validation result

The two-phase Poiseuille flow problem is the second problem analyzed to validate the results. In this problem, the fluid inside a channel with 50% saturation has been investigated according to Figure (4). The speed profile obtained from the simulations is compared with the analytical relations presented in equation (22) in figure (5).

$$u(y) = -\frac{\Delta P}{2L\mu_w}\left(b^2 - y^2\right), |a| \le |y| \le b;$$
$$u(y) = -\frac{\Delta P}{2L\mu_w}\left(b^2 - a^2\right) - \frac{\Delta P}{2L\mu_{nw}}\left(a^2 - y^2\right), |0| \le |y| \le a; \tag{22}$$

The quantity that is important in this problem is the saturation volume (S_w). This quantity is defined as the ratio between the volume occupied by the wetting phase (w) and the total volume of the channel according to Eq. (23). Figure (5) compares the results of the simulations carried out in this research with the analytical solution presented in Eq. (22).

$$S_w = \frac{V_w}{V_w + V_{nw}} \tag{23}$$

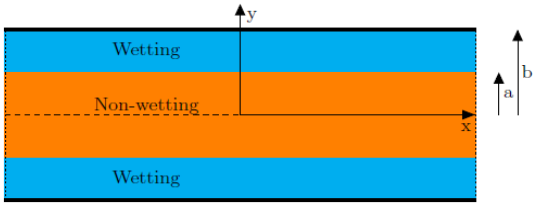

Figure 4: Geometry of two-phase Poiseuille flow problem.

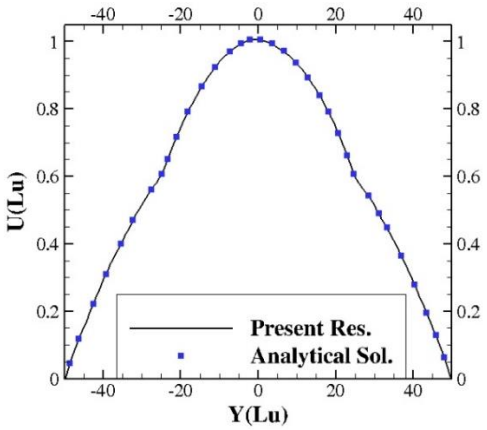

Figure 5: Two-phase Poiseuille flow validation results.

Results and discussion

In this section, the results related to the dynamics of single droplet of the same size as solid particles inside the porous medium are presented. In the range of dimensionless numbers studied in this research, two phenomena may occur when the droplet collide with the particles of the porous medium. It either may stops behind the obstacles or broken by the obstacles. Figures 6-7 show how the droplet breaks

up or stops for different conditions presented in Table 1. Figure 6 is related to the condition (a) that leads to the droplet confinement and Figure 7 is related to the condition (b) that leads to the drop breaking. According to more details in the drop breaking process, the number of snapshots presented in Figure 7 is more than Figure 6. As shown in Figure 6, the fluid flow pushes the drop to the central particle. Since the flow does not have enough energy to overcome the surface tension force in this case, it cannot breaks up the droplet.

By increasing the capillary number in the second case (Figure 7), the speed of fluid flow increases. The increase in kinetic energy of the flow leads to compression, spreading and finally breakup of the droplet it into three parts. As indicated in this figure, one part is trapped behind the central particle and the other two parts flow around it. Due to the periodic boundary condition in the streamwise direction, two separated drops alternately exit from one side of the computational domain and enter from the opposite side.

Table 1: Flow conditions related to Figs. 6 and 7.

	None. Dim. Press. Ratio	Ca	Ohn	Density Ratio
a	1.08×10^{-4}	0.0561	0.3138	1/3
b	1.44×10^{-4}	0.2374	0.4438	1/2

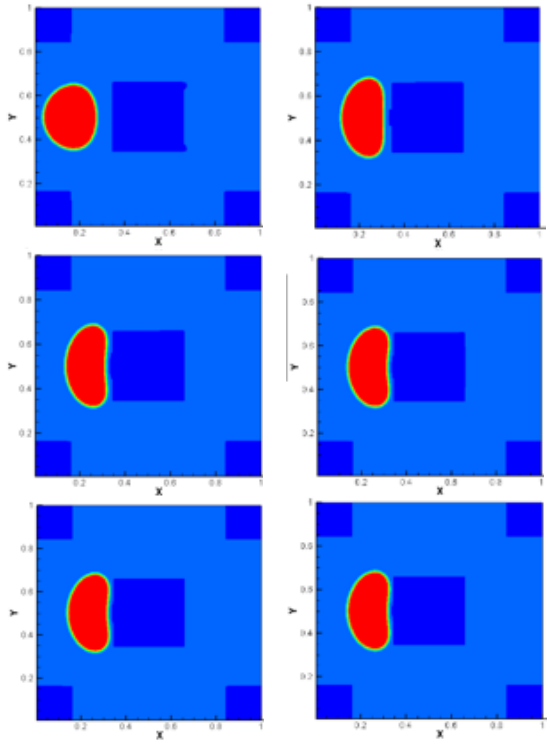

Figure 6: Droplet trapping behind the central particle for case a from Table 1

In Figures. 8 to 13 changes of flow Reynolds number as a function of Ohnesorge number for different dimensionless body forces are shown. Factors affecting the Reynolds number in the porous medium are: geometry of the porous medium, pressure gradient and droplet dynamics. In order to check the above, simulations performed for three values of dimensionless body force, two different density ratios of 1:2 and 1:3, and three different porosity values. The most important results obtained from these simulations are presented as follows.

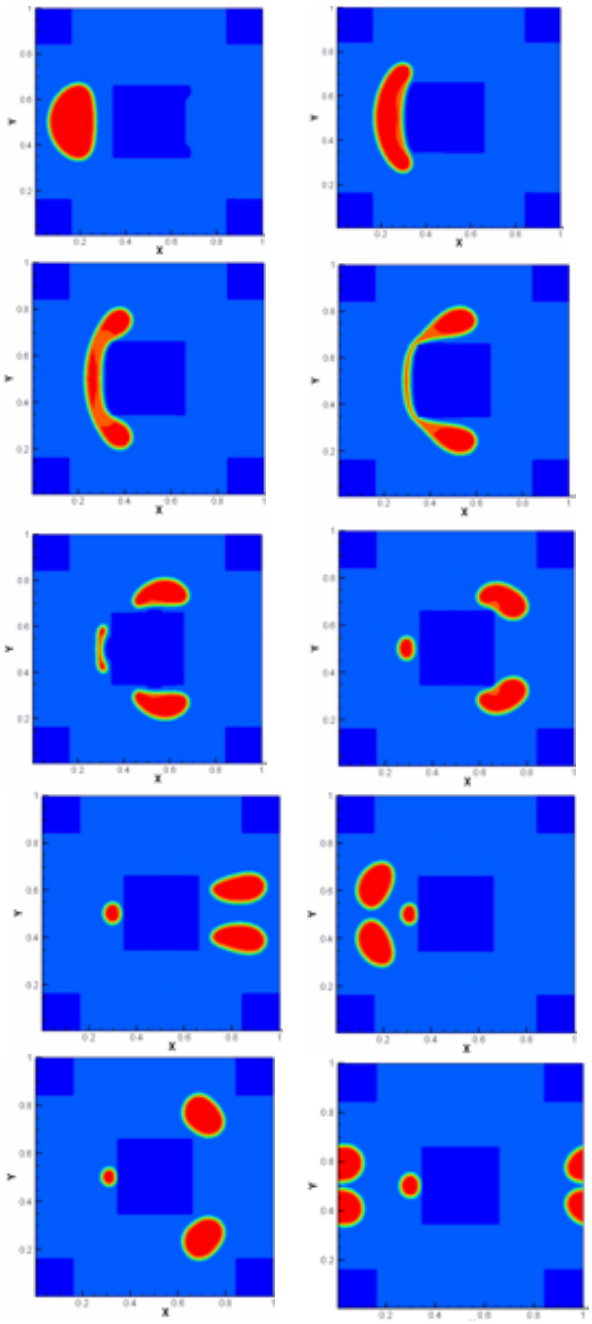

Figure 7: Droplet breakup for case b from Table 1

According to these figures, there is a critical Ohnesorge value that the Reynolds number of the flow suddenly increases after passing through it. In other words, for Ohnesorge lower than this critical value, less flow passes through the porous medium and as a result, the Reynolds number of the flow is lower. However, with the increase of Ohnesorge number from this value, it is as if a barrier is removed from the flow path and as a result more flow passes through the porous medium. From the physical point of view, the critical Ohnesorge number is related to the breakup of the droplet. Thus, for smaller values of Ohnesorge number, the drop maintains its integrity and acts like a barrier against the flow. As the Ohnesorge number increases, the drop gradually loses its integrity. Therefore, it first expands on the central particle and then it is broken and washed away by the fluid flow. This process is associated with an increase in the flow rate of the fluid passing through the porous medium and as a result the Reynolds number of the flow.

As indicated in Figure 13-8, with the increase of the dimensionless body force, we always see an increase in the mass flow rate and as a result the Reynolds number. The reason for this issue is also clear due to the increase in fluid driving force. In addition, it can be seen that with the increase of the dimensionless body force, the critical Ohnesorge number decreases in all cases. This issue is also expected considering the effect of body force on the increase of fluid kinetic energy. As the kinetic energy of the flow increases, the shear force transferred from the fluid to the droplet increases, which causes the droplet to break up earlier.

Based on Figures 13-8, it can be seen that the porosity coefficient has the same effects as the dimensionless body force. As the porosity coefficient increases, the Reynolds number increases, but the critical Ohnesorge number decreases. Because by increasing the porosity coefficient, there is more space for the fluid to pass and as a result, the blocking effects of the porous medium are reduced. By reducing the resistance of the porous medium to the flow of the fluid, the flow rate and as a result the Reynolds number increases. As the Reynolds number of the flow increases, the kinetic energy of the flow also increases, which causes the droplet to break up faster at lower Ohnsurge numbers.

Variations in capillary number with respect to Ohnsurge number for different density ratios and dimensionless body forces are shown in Figures 14-16 for different porosity coefficients. The diagrams in Figure 14 correspond to the porosity coefficient of 0.75, the diagrams in Figure 15 correspond to the porosity coefficient of 0.8, and the diagrams in Figure 16 correspond to the porosity coefficient of 0.85. Abbreviations BU and T in these figures refer to the drop breaking and trapping, respectively.

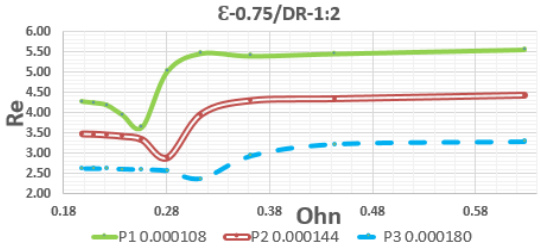

Figure 8: Ohnesorge -Reynolds diagram for density ratio 1:2 and porosity coefficient 0.75.

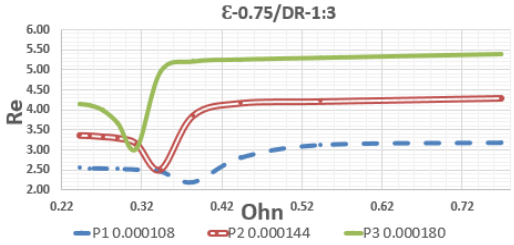

Figure 9: Ohnesorge -Reynolds diagram for density ratio 1:3 and porosity coefficient 0.75.

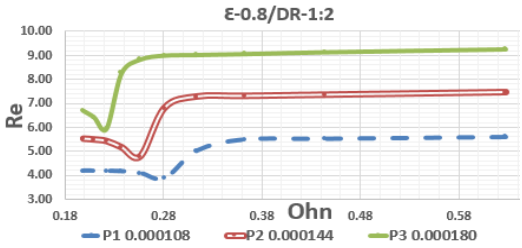

Figure 10: Ohnesorge -Reynolds diagram for density ratio 1:2 and porosity coefficient 0.8.

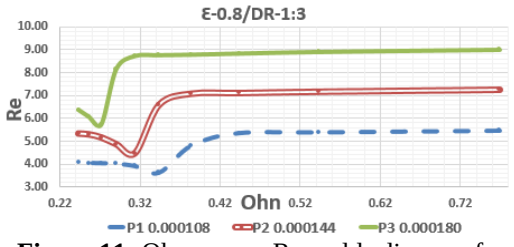

Figure 11: Ohnesorge -Reynolds diagram for density ratio 1:3 and porosity coefficient 0.8.

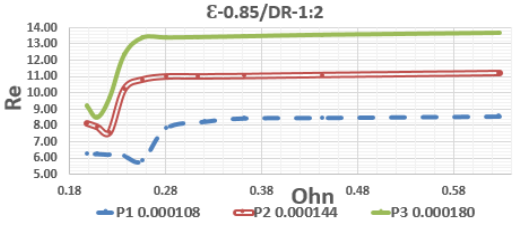

Figure 12: Ohnesorge -Reynolds diagram for density ratio 1:2 and porosity coefficient 0.85.

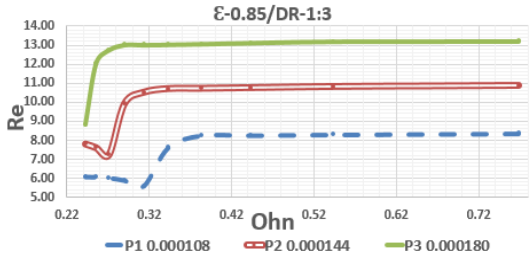

Figure 13: Ohnesorge -Reynolds diagram for density ratio 1:3 and porosity coefficient 0.85.

The droplet dynamics are shown in Figures 14-16 for two density ratios of 1:2 and 1:3 and three dimensionless body forces of 1.08×10^{-4}, 1.44×10^{-4} and 1.80×10^{-4} (with abbreviations P1, P2 and P3). The red part of the graphs in these figures is related to the conditions of droplet confinement, and the black part is related to the droplet breakage.

As in graphs of all three figures 14 to 16, the breakup of drops in the range of dimensionless numbers investigated in this article occurs around the Capillary number of 0.1. Therefore, this number can be considered as a critical value for the breakup of drops in the range of dimensionless numbers investigated in this research. Also, it can be seen that with the increase of the density ratio, the critical Ohnesorge number in which the droplet breakup occurs increases. Since the square root of the droplet density enters in the denominator of the Ohnesorge number, it is natural that with the increase of the density ratio, the droplet breakup occurs at higher Ohnesorge numbers.

Another point that is noticeable in the graphs of figures 14 to 16 is the effect of the porosity coefficient in increasing the slope of the variation of the capillary number whit respect to the Ohnesorge number. The reason for the increase in the slope is that with the increase in the porosity coefficient, the mean velocity of the two-phase flow increases. As the flow rate increases, the capillary number is also increases.

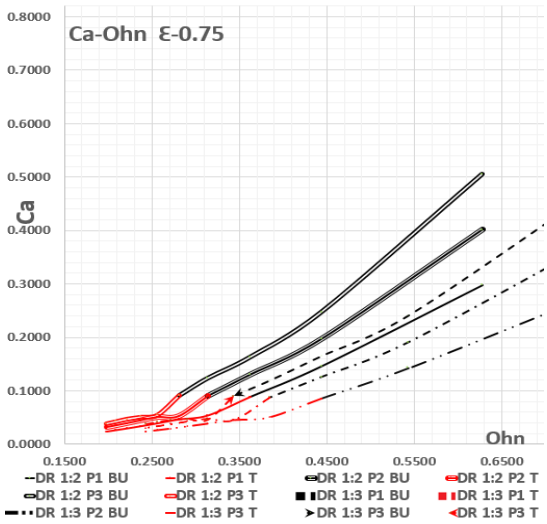

Figure 14: Ohnesorge-capillary diagram for density ratio 1:2 and 1:3 and porosity 0.75.

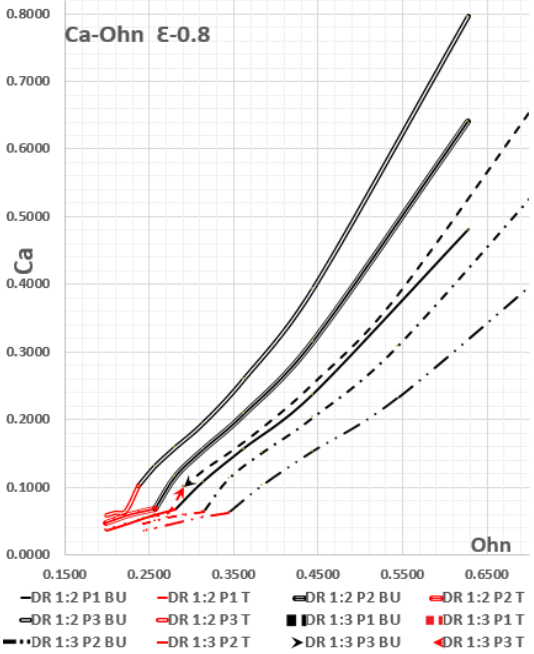

Figure 15: Ohnesorge-capillary diagram for density ratio 1:2 and 1:3 and porosity 0.8.

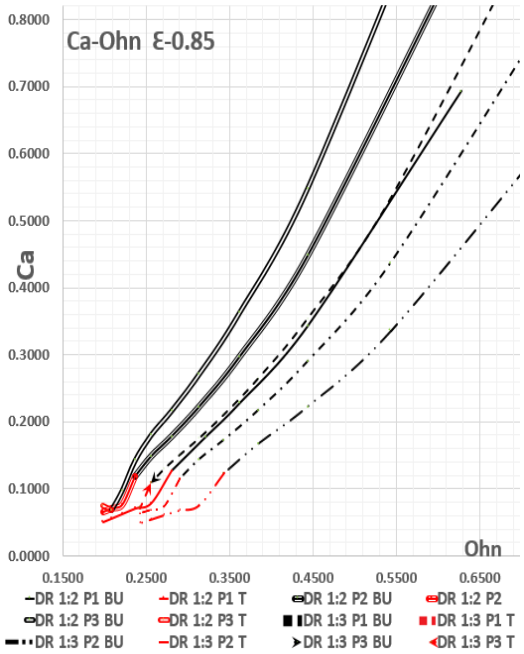

Figure 16: Ohnesorge-capillary diagram for density ratio 1:2 and 1:3 and porosity 0.85.

In addition, it can be seen that with increasing porosity, the relative fraction of droplet breakup modes to droplet confinement mode (red areas in the curves) increases. Of course, this issue was expected due to the effect of greater porosity on the easy flow of fluid inside the porous medium and the increase in flow energy in breaking the droplets.

Conclusion

In this article, the dynamics of a droplet of the same size as the particles forming a porous medium was investigated. In order to identify the breakup behavior of the drop inside the porous medium, various dimensionless numbers such as Capillary, Ohnesorge, porosity and dimensionless body force were investigated. In the range of dimensionless numbers studied, two physics of breakup and trapped drop were observed. It was shown that there is a critical Ohnesorge number, which the drop breaks for values greater than that. Also, it was observed that this critical value decreases with the increase of dimensionless body force and porosity coefficient. The results show that with the breaking of the droplet, the fluid mass flow rate and consequently the flow Reynolds number increases.
In addition, Reynolds-Ohnesorge and Capillary-Ohnesorge diagrams were presented in order to predict the droplet behavior at different porosity coefficients. In these diagrams, the ranges related to the trapping and breaking of droplets were determined, which can provide useful information regarding the studied two-phase flow phenomenology.

References

[1] Dullien, F.A.L (1991) Porous Media, Fluid Transport and Pore Structure, San Diego, Academic Press.

[2] V. Chilingarian, Erle C. Donaldson, George, and Yen, Teh Fu (1985) Enhanced Oil Recovery, I Fundamentals and Analyses, Elsevier.

[3] Ingham, D.B. and Pop, I. (2002) Transport Phenomena in Porous Media II, Oxford, Pergamon Press.

[4] Khaled, A.R.A. and Vafai, K. (2003) The role of porous media in modeling flow and heat transfer in biological tissues, Int J Heat Mass Transf, 46(26): 4989-5003.

[5] Rowlinson, J.S. and Widom, B. (2011) Porous media, Applications in Biological Systems and Biotechnology, Boca Raton, Crc Press Taylor & Francis Group.

[6] Pan, C., Luo, L.-S., and Miller, C.T. (2006) An evaluation of lattice Boltzmann schemes for porous medium flow simulation, Comput Fluids, 35:898-909.

[7] Aaltosalmi, U. (2005) Fluid Flow in Porous Media with the Lattice-Boltzmann Method, PhD Thesis, Department of Physics, University of Jyväskylä.

[8] Rostamzadeh, H., Salimi, M. R., & Taeibi-Rahni, M. (2018). Permeability correlation with porosity and Knudsen number for rarefied gas flow in Sierpinski carpets, Journal of Natural Gas Science and Engineering, 56, 549-567.

[9] Rostamzadeh, H., M. R. Salimi, and M. Taeibi-Rahni. (2019) Pore-scale modeling of rarefied gas flow in fractal micro-porous media, using lattice Boltzmann method (LBM), Journal of Thermal Analysis and Calorimetry 135(3),1931-1942.

[10] Gunstensen, Andrew K. and Rothman, Daniel H. (1993) Lattice-Boltzmann studies of immiscible two-Phase flow through porous media, J. Geophys. Res., 98:6431-6441.

[11] Ferreol, Bruno, and Rothman, Daniel H. (1995) Lattice Boltzmann simulations of flow through fontainebleau sandstone, Transport in Porous Media, 20(1): 3-20.

[12] Martys, Nicos S. and Chen, Hudong (1996) Simulation of multi-component fluids in complex three-dimensional geometries by the lattice Boltzmann method, Phys Rev E Stat Nonlin Soft Matter Phys, 53.

[13] Tölke, Jonas, Krafczyk, Manfred, Schulz, Manuel, and Rank, Ernst (2002) Lattice Boltzmann simulations of binary fluid flow through porous media, Philos Trans R Soc Lond A, 360:535–545.

[14] He, X., Chen, S., Zhang, R, (1999) A Lattice Boltzmann Scheme for Incompressible Multiphase Flow and Its Application in Simulation of Rayleigh– Taylor Instability, Journal of Computational Physics, 152(2) 642-663.

[15] Lin, C.L., Videla, A.R., and Miller, J.D. (2010) Advanced three-dimensional multiphase flow simulation in porous media reconstructed from X-ray microtomography using the He Chen Zhang lattice Boltzmann model, Flow Measurement and Instrumentation, 21:255-261.

[16] Frank, X. and Perré, P. (2012) Droplet spreading on a porous surface, A lattice Boltzmann study, Physics of Fluids, 24.

[17] Shan, X. and Chen, H., (1993) Lattice Boltzmann model for simulating flows with multiple phases and components, Phys. Rev. E 47, 1815.

[18] Huang, H., Li, Z., Shuaishuai, L., and Lu, X. (2009) Shan-and-Chen-type multiphase lattice Boltzmann study of viscous coupling effects for two-Phase flow in porous media, Int J Numer Methods Fluids, 61:341-354,.

[19] Pan, C., Hilpert, M., and Miller, C.T. (2004) Lattice-Boltzmann simulation of two-phase flow in porous media, Water Resour Res, 40(1).

[20] Hao, L. and Cheng, P. (2010) Pore-scale simulations on relative permeabilities of porous media by lattice Boltzmann method, Int J Heat Mass Transf, 53:1908-1913.

[21] Tabe, Yukata, Yongju, Lee, Takemi, Chikahisa, and Masaya, Kozakai (2009) Numerical simulation of liquid water and gas flow in a channel and simplified gas diffusion layer model of polymer electrolyte membrane fuel cell using the lattice Boltzmann method, J Power Sources, 193.

[22] Huang, Haibo, Huan, Jun-Jie, and Lu, Xi-Yun (2014) Study of immiscible displacements in porous media using a color-gradient-based multiphase lattice Boltzmann method, Comput Fluids, 93:164-172.

[23] Huan, Haibo, Wang, Lei, and Lu, Xi-Yun (2011) Evaluation of three lattice Boltzmann models for multiphase flows in porous media, Comput Math Appl, 61:606–3617.

[24] Liu, H., Valocchi, A. J., Kang, Q., and Werth, C. (2013) Pore-scale simulations of gas displacing liquid in a homogeneous pore network using the lattice Boltzmann method, Transport in Porous Media, 99:555-580.

[25] Latifiyan, Navid, Farhadzadeh, Mohsen, Hanafizadeh, Pedram, and Rahimian, Mohammad Hassan (2015) Numerical study of droplet evaporation in contact with hot porous surface using lattice Boltzmann method, International Communications in Heat and Mass Transfer, 71: 56 –74 .

[26] Taghilu, M. and Rahimian, M. H. (2013) Simulation of 2d droplet penetration in porous media using lattice Boltzmann method, Modares Mechanical Engineering, 13:43-56 (in Persian).

[27] SalehAbadi, H., Nazari, M., Kayhani, M.H., (2017) Simulation of Two Phase Penetration and Routing the fluid in a Specified Path in Layered Porous Media with Lattice Boltzmann Method, Tabriz Mech. Eng.,14,3: 129-138 (in Persian).

[28] Rastegar Rajeouni, P., and Rahmati, A.R., (2021) Simulation of Deformation and Break-up of Droplets in the Presense of Electric Field in Porous Media Using Lattice Boltzmann Method, Journal of Numerical Methods in Engineering,40,1: 79-101 (in Persian).

[29] Javadi, A., Bastani, D., Taeibi-Rahni, M., and Javadi, Kh. (2006) The effects of hydrodynamics characteristics on the mass transfer during droplet formation using computational approach, ASME's International Mechanical Engineering Congress and Exposition (IMECE), 811-821.

[30] Chen, F. and Hagen, H. (2011) A survey of interface tracking methods in multi-phase fluid visualization, Visualization of Large and Unstructured Data Sets - Applications in Geospatial Planning, Modeling and Engineering (Irtg 1131 Workshop), 19:11-19.

[31] Cooper-White, J.J., Fagan, J.E., Tirtaatmadja, V., Lester, D.R., and Boger, D.V (2002) Drop formation dynamics of constant low-viscosity, J Nonnewton Fluid Mech, 106:29-59.